

Study of nanoimprint pattern transfer on hydrogen silsesquioxane

Sun Zen Chen^{a)}

Center for Nano-Science and Technology, University System of Taiwan, National Tsing Hua University, Hsinchu, Taiwan, Republic of China

Jen Fu Liu

Institute of Electronics Engineering, National Tsing Hua University, Hsinchu, Taiwan, Republic of China

Henry J. H. Chen

Department of Electrical Engineering, National Chi Nan University, Nantou, Taiwan, Republic of China

Fon Shan Huang

Institute of Electronics Engineering, National Tsing Hua University, Hsinchu, Taiwan, Republic of China

(Received 21 June 2005; accepted 15 June 2006; published 18 July 2006)

The effects of process parameters on pattern embossing into hydrogen silsesquioxane films and the pattern degradation of hydrogen silsesquioxane were investigated. Methylisobutylketone (MIBK) was used to dilute hydrogen silsesquioxane, and NX-1000 (Nanonex) was used to imprint hydrogen silsesquioxane embossed with a Si grating mold at 25°–180 °C under 2–2.5 MPa. The imprint results were observed by scanning electron microscopy and correlated to the analysis results of Fourier transform infrared spectroscopy (FTIR) and nanoindentation. The FTIR results show that network-type bonding was promoted by dilution with MIBK and increasing baking temperatures from 50 °C to 180 °C. High-temperature thermal-cycle heat treatment can promote the formation of network bonds, which make hydrogen silsesquioxane film undergo plastic deformation more easily. In contrast, low-temperature thermal-cycle heat treatment can result in hydrogen silsesquioxane having a highly viscous response and high time-dependent deformation behavior. The diluted hydrogen silsesquioxane film under prebaking at 150 °C for 3 min and imprinting at 180 °C for 2 min under 2.5 MPa resulted in a high-fidelity pattern replication without pattern degradation after aging at room temperature for 20 days. © 2006 American Vacuum Society. [DOI: 10.1116/1.2221314]

I. INTRODUCTION

Photolithography has been the patterning technology for manufacturing integrated circuits. However, due to the diffraction limit, there are no expectations that sub-100 nm features will be easily patterned by traditional photolithography. Therefore, nanofabrication technologies are indispensable techniques for making sub-100 nm features. Nanoimprint lithography (NIL) is a very useful lithography technique to make nanostructure devices with high resolution and low cost,¹ and it is regarded as one of the ten emerging technologies likely to change the world.²

The principle of nanoimprint lithography is quite simple. In this method, a mold with engraved patterns is mechanically pressed onto a substrate coated with a resist material [such as polymethyl methacrylate (PMMA)] at certain temperature and pressure conditions. This compression leaves the “negative” of the mold patterns in the resist when the pressure is released and the mold is lifted. The resist layer having this thickness contrast, which the photolithography essentially does, thereby realizes the pattern transfer onto the substrate. PMMA is the most used material as a NIL replication resist. Recently, some resist materials have been proposed to replace PMMA, such as hydrogen silsesquioxane (HSQ).

Morita *et al.*³ used a three-dimensional (3D) nanoimprint diamondlike carbon mold (170 nm in linewidth, 640 nm in space, and 410 nm in height) fabricated by focused-ion-beam CVD to imprint 0.3 μm thick HSQ. The imprint pressure was set from 2.5 to 4.5 MPa for 1 min at room temperature. The transferred line pattern of HSQ was 250 nm in width and 450 nm in height. Matsui *et al.*⁴ proposed room-temperature NIL using HSQ as a replicated material. The replicated nanoscale patterns of holes (90 nm diameter and 600 nm pitch) and lines (50 nm linewidth and 200 nm pitch) were obtained after being impressed at 4.0 MPa for 1 min, pre-baked at 50 °C for 20 min. Although Matsui *et al.* had imprinted nanoscaled patterns at room temperature, they did not report the difference between the mold and imprinted HSQ.

Sikder *et al.*^{5,6} used a nanoindentation technique with a continuous-stiffness-measurement (CSM) method to test the mechanical properties of low dielectric constant materials. They suggested that the weak mechanical integrity of spin-on siloxane polymers could be regarded as soft polymerlike materials that have time-dependent behaviors. Oyen *et al.*⁷ developed a viscous-elastic-plastic (VEP) model to describe the sharp indentation behaviors of time-dependent materials. The VEP model was constructed from a series of independent quadratic mechanical elements, with viscous, elastic, and plastic responses. A series combination of these

^{a)}Electronic mail: szchen@mx.nthu.edu.tw

TABLE I. Compositions and process parameters of samples used for FTIR and nanoindentation tests.

Sample code	HSQ:MIBK	Film thickness (Å)	Temperature (°C)	Time (min)
A150	2:1	4000	150	3
B050	4:5	2380	50	3
B150	4:5	2380	150	3
B180	4:5	2380	180	3

three elements gave a total displacement arising from the sum of displacements in the individual elements.

As discussed above, HSQ has been demonstrated as a useful NIL resist for its superior properties. However, the fidelity between mold and imprinted HSQ patterns has not been studied. The relationship between the properties and imprinted results of HSQ has also not been studied. And there is still no research investigating the effects of room-temperature aging on imprinted HSQ patterns. In this paper, we focus on the effects of process parameters on properties of HSQ and pattern embossing into HSQ films. Fourier transform infrared spectroscopy (FTIR) is used to observe the chemical structures of HSQ. To investigate the relationship between deformation behaviors and imprinted results of HSQ, we use continuous-stiffness-measurement and load-unload methods to investigate mechanical properties. Various sequences of processes were performed in order to get a fidelity pattern transfer. Another objective of our work is to determine the pattern degradation of HSQ films for room-temperature aging effects. The nondegradation plastic deformation will be related to hardness, viscosity, and thermal stability of the HSQ.

II. EXPERIMENTS AND METHODS

Table I lists compositions and process parameters of HSQ prepared for FTIR and nanoindentation tests. HSQ (FOx15, Dow Corning Corporation) was mixed with MIBK in a ratio of 2:1 or 4:5 and stirred for 2 h. The solid content of the solutions is about 14.7 wt. % and about 9.8 wt. %, respectively. Before coating with HSQ, the silicon wafers were cleaned using the RCA process and then dried with N₂. The HSQ solution was spun onto silicon wafers in two steps: 1000 rpm for 10 s and then 6000 rpm for 20 s. HSQ films were then prebaked at 50 °C or 150 °C for 3 min on a hot plate.

The chemical structures of HSQ films were investigated by FTIR using reflected mode. The mechanical properties of HSQ films were measured by a nanoindenter (MTS nanoindenter XP system, MTS Systems Corporation, USA) with a diamond Berkovich indentation tip. Two test methods, “CSM” and “load-unload,” were adopted to measure the mechanical properties of the HSQ films. The CSM method is used for measuring absolute and depth-dependent hardness values of HSQ. The load-unload technique is used to manifest the viscous response of HSQ.

The CSM method was carried out in the following sequence: The indenter approached the surface at a rate of 10 nm/s until contact was detected; this was followed by a loading segment with a constant strain rate of 0.05 s⁻¹ to a predefined maximum depth (50 nm); the load at this maximum depth was held constant for 10 s; the indenter was then withdrawn from the sample at the same rate as loading. The hardness values were calculated by averaging a number of separate indentations at particular depth specifications. The load-unload experiments were performed by indenting HSQ at a maximum load (0.003 g) within 45 or 15 s, then holding at a peak load for 300, 135, 10, or 0.1 s, and finally, withdrawing from the sample at the same rate as loading.

Table II lists compositions and process parameters of HSQ prepared for the imprinting study. HSQ was mixed with MIBK in a ratio of 2:1 or 4:5 and stirred for 2 h. The solid content of the solutions is about 14.7 wt. % and about 9.8 wt. %, respectively. Before coating with HSQ, 6 inch silicon wafers were cleaned using the RCA process and then dried with N₂. A 6 inch silicon mold, which had a pattern of grating lines (56 nm in width, 72 nm in depth) was provided by Nanonex. Before imprinting, the mold was first cleaned in acetone and dried with N₂. Imprinting of HSQ was conducted using NX-1000 (Nanonex, USA). After vacuuming the chamber, the pre-press pressure was set as 0.8 MPa by

TABLE II. Sample compositions and process parameters for imprint tests.

Sample code	HSQ:MIBK	Film thickness (Å)	Prebake temperature (°C)	Imprint pressure (MPa)	Imprint temperature (°C)
A150-25-130	2:1	4000	150	2.5	130
B150-25-130	4:5	2380	150	2.5	130
B150-25-180	4:5	2380	150	2.5	180
B150-20-180	4:5	2380	150	2.0	180
B050-25-025	4:5	2380	50	2.5	25

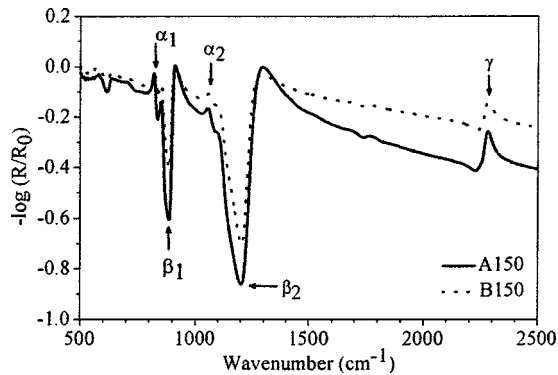


FIG. 1. Reflectance FTIR for samples A150 and B150.

introducing Ar into the chamber during heating. Once the predetermined temperature (25 °C, 130 °C, or 180 °C) is reached, the imprint press pressure was rapidly raised to 2.0 or 2.5 MPa within 10 s and kept for 2 min; this was followed by cooling to room temperature (about 15 s) and then releasing the press pressure.

A Hitachi S-4000 scanning electron microscopy (SEM) was used to examine the pattern replication of the imprinted HSQ. After being aged at room temperature for several days, the imprinted HSQ was observed again by SEM to check the pattern degradation.

III. RESULTS AND DISCUSSIONS

Figures 1 and 2 show the chemical structures of HSQ films measured by reflectance FTIR. The sample compositions and process parameters are listed in Table I. Figure 1 describes the structural changes derived from the dilution with MIBK. Figure 2 shows the FTIR peak changes caused by heat treatments. Table III lists the characteristic structures for HSQ film as shown in Figs. 1 and 2. α_1 and α_2 represent the network bonding, where β_1 and β_2 are the cage-like bonding.⁸

As shown in Fig. 1, the network characteristic Si-O peaks (α_1 and α_2) of samples A150 and B150 show small differences in areas; but the cage-like characteristic Si-O peaks (β_1 and β_2) of sample A150 are significant larger than sample B150. This result suggests that the A samples are more cage-like than for B samples. This means that dilution with MIBK

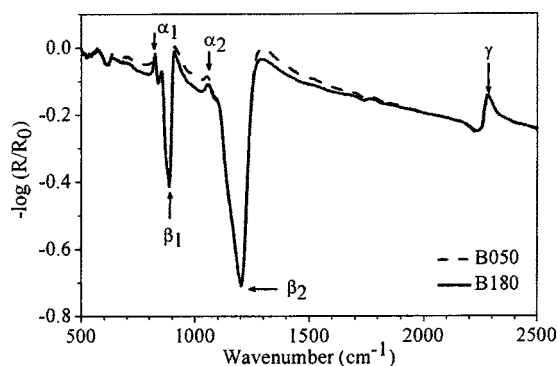


FIG. 2. Reflectance FTIR for samples B050 and B180.

TABLE III. FTIR characteristic chemical bonding of HSQ.

Symbol	Bonding structure	Wavenumber (cm ⁻¹)
α_1	Network Si-O bending	822
β_1	Cage-like Si-O bending	881
α_2	Network Si-O stretching	1064
β_2	Cage-like Si-O stretching	1175
γ	Si-H	2250

affects not only the film thickness of HSQ, but also, the chemical structures that are responsible for mechanical properties. In Fig. 2, samples B180 and B050 also differ in the two characteristic bond peaks. Although the peak intensities of β values seem to be almost the same for B050 and B180, the α values of B180 show higher peak intensity than for B050. This result indicates that the network-type bonding is promoted as baking temperatures increase from 50 °C to 180 °C. This difference in chemical structures is responsible for the mechanical properties and imprinting results, as will be discussed below.

Figure 3 shows the typical indentation results for the CSM method (0.05 s⁻¹ strain rate and holding at a maximum load for 10 s) of HSQ baked at 50 °C–180 °C for 3 min. Figure 3(a) is a plot of load versus penetration depth, and Fig. 3(b) is the calculated depth-dependent hardness. The hardness is obtained in the penetration depth range from 10 to 30 nm to minimize substrate effects. Table IV summarizes the average values of 7–10 measurements. As listed in Table IV, the averaged hardness values of sample A150 is

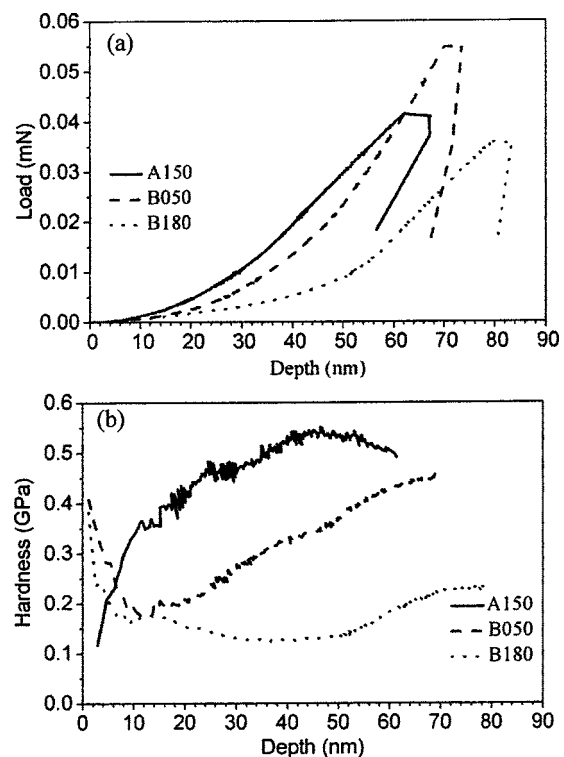


FIG. 3. Indentation curves of (a) load vs depth (b) hardness vs depth measured by CSM method for samples A150, B050, and B180.

TABLE IV. Hardness of HSQ films derived from CSM method.

Sample code	Hardness (GPa)
A150	0.565 ± 0.122
B050	0.203 ± 0.032
B180	0.159 ± 0.019

the largest (0.565 ± 0.122 GPa) and sample B180 is the smallest (0.159 ± 0.019 GPa). The low hardness of sample B180 suggests that it may be easy to deform HSQ after dilution with MIBK and baking at 180°C . Another interesting result shown in Fig. 3(a) is that the indentation depth increases with holding time at maximum load. This creep phenomenon under hold periods at maximum load is a characteristic of time-dependent materials, which was also observed by Sikder *et al.*^{5,6} The time-dependent characteristics are caused by a viscous response of materials as discussed for the VEP model.⁷ These time-dependent materials will exhibit different hardnesses while the holding time or load changes. Because the data are not taken at the equilibrium state, the CSM results of Table IV provide qualitative comparisons of the hardness values of various HSQ films.

Figure 4 are the test results for the load-unload test method. We believe this measurement helps us to understand the plastic deformation and VEP model. Figure 4(a) shows the load-displacement curves of samples indented at 0.003 g for 300 s with constant load and unload rate ($0.003\text{ g}/45\text{ s}$). Figure 4(b) describes the creep phenomena during 300 s holding periods of samples shown in Fig. 4(a). The creep displacements are referenced to the initial displacements at peak load. Figure 4(c) compares the indentation results between samples A150 and B180 for different hold periods (135 , 10 , and 0.1 s) at constant load and unload rate ($0.003\text{ g}/15\text{ s}$). As shown in Fig. 4(a), the different behaviors of samples are caused by the different process treatments. The load-unload curves of the samples show two interesting results. The first is that the creep rate of samples held at peak load for 300 s can be divided into two segments, as shown in Fig. 4(b). The second is that the unloading slope of samples are nearly to vertical, which implies a perfectly plastic deformation. So, after being held for 300 s , the samples deform plastically. The sample shows different plasticity for various holding times, which will be discussed in Fig. 4(c).

In Fig. 4(b), the creep rate changes with holding time; eventually, the creep rate reaches a steady state, which remains essentially constant at the end of hold periods. Table V lists the creep rates derived from Fig. 4(b). The steady-state creep rate is about 0.047 nm/s for sample A150, 0.043 nm/s for sample B050, and 0.017 nm/s for sample B180. As suggested by the VEP model,⁷ the steady-state creep rate is the reciprocal of the root of the viscosity, which is responsible for the time-dependent response. Therefore, the rank of viscous coefficient values of the samples is $A150 < B050 < B180$. For larger viscosity levels, as in the cases of sample

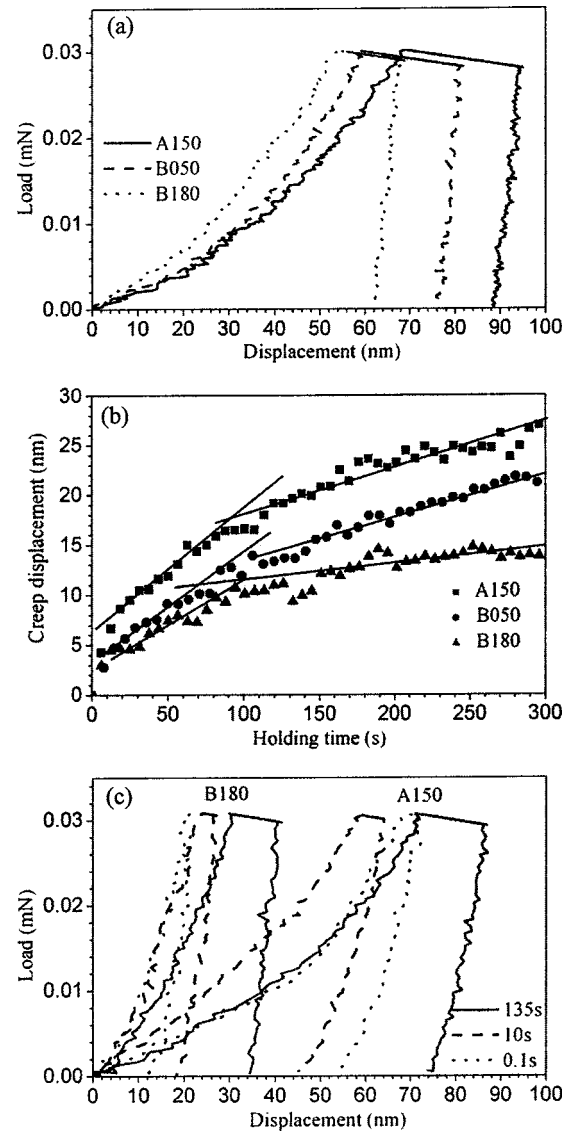


FIG. 4. (a) Load-displacement and (b) creep displacement-time responses for load-unload indentation creep experiments on samples A150, B050, and B180 holding at maximum load for 300 s . (c) load-unload indentation results of samples A150 and B180 for different maximum load holding time (135 , 10 , and 0.1 s).

B180, the time-dependence behavior is reduced, and the total VEP response is much nearer to a purely elastic-plastic response.

In Fig. 4(c), the unloading slopes of sample B180 for different hold periods are all very close to a vertical line. This means that 135 s of holding time is enough to make

TABLE V. Creep rate of load-unload indentation tests during holding at maximum load for 300 s at a load rate of $0.003\text{ s}/45\text{ s}$.

Sample	Initial creep rate (nm/s)	Steady-state creep rate (nm/s)
A150	0.124	0.047
B050	0.110	0.043
B180	0.090	0.017

TABLE VI. Characteristics of mold pattern and imprinted HSQ films.

Code	Width (nm)	Depth (nm)
Mold	56	72
A150-25-130	40.2	31.4
B150-25-130	40.2	58.5
B150-25-180	58.1	74.1
B150-20-180	42.9	22.9
B050-25-025	41.5	N.A.

sample B180 deform plastically. After being held for 135 s at a load of 0.003 g, the unloading slope of sample A150 is still not as vertical as that of sample B180. The unloading slope of sample A150, which increases with peak load hold periods, shows that the mechanical deformation of sample A150 is dominated by a viscous response and is highly time-dependent. Comparing the unloading slope of sample A with that of sample B also verifies that sample B has a higher viscosity than sample A.

As shown in the test results of the CSM and load-unload methods, sample B180 demonstrates lower hardness, less viscous response, and higher plastic deformation among the samples. This means that dilution with MIBK and baking at higher process temperature, as in the case of sample B180, makes HSQ films demonstrate plastic deformation more easily than other films. These changes of mechanical properties could be correlated to the forming of network structures of HSQ. In the following paragraphs, we will show that these changes of mechanical properties and chemical structures are responsible for the imprint results.

Table II lists the sample compositions and process parameters of HSQ for imprint tests. Table VI summarizes the average width and depth of imprinted HSQ observed by SEM within one day after imprinting. Figure 5 shows some representative SEM micrographs. According to the SEM observations, sample A150-25-130 and sample B150-25-130 have the same replication width (40.2 nm), but the imprinted depth of sample B150-25-130 is deeper than sample A150-25-130. As discussed above, the FTIR chemical analysis shows that sample A150 is more cagelike than sample B150. The nanoindentation results show that A samples have higher hardness, but higher viscous response with less plasticity, than B samples. This is why sample B150-25-130 has a deeper imprinted depth than sample A150-25-130. This result suggests that the dilution of HSQ affects not only the film thickness, but also, the pattern transfer, which is deduced from the changes of chemical structures and mechanical properties.

The imprint depth of sample B150-25-130 of only 58.5 nm means that the imprinted temperature at 130 °C is too low. So, raising the imprint temperature to 180 °C is necessary. The replication of sample B150-25-180 is 58.1 nm in width and 74.1 in depth. It has almost the same pattern as the mold. By decreasing the imprint pressure to 2.0 MPa, sample B150-20-180 shows only 22.9 nm in depth and 42.9 nm in width. This implies that imprinting under a

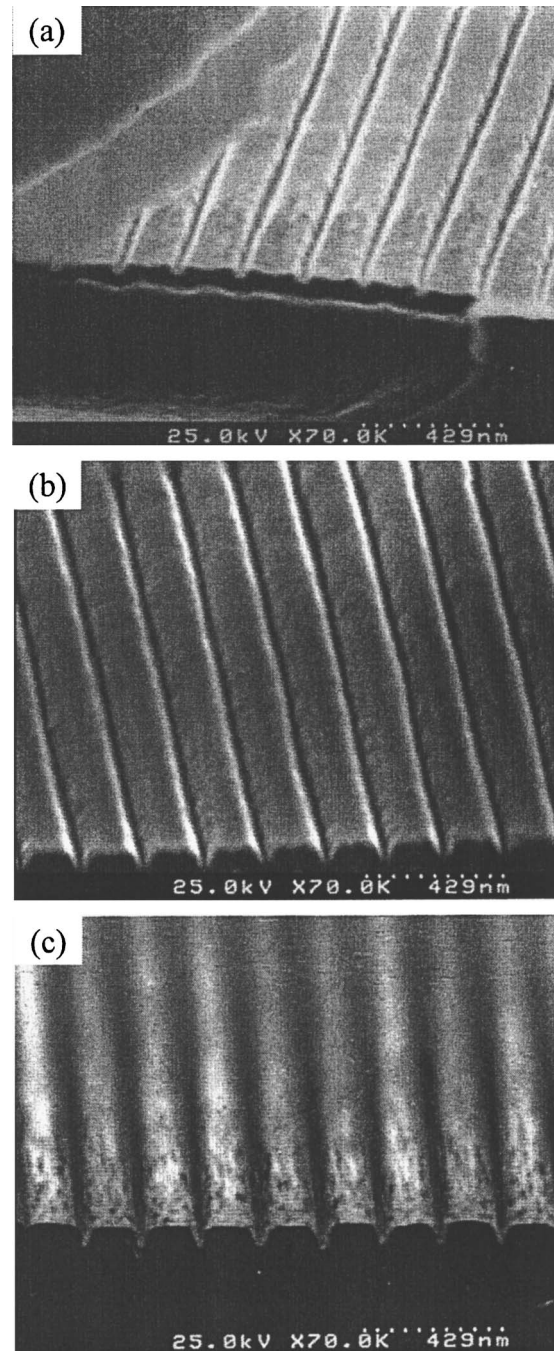


FIG. 5. 45°-tilted SEM micrographs of samples (a) A150-25-130, (b) B150-25-130, and (c) B150-25-180.

pressure of 2 MPa is not enough for the imprint process. For room-temperature imprinting, sample B050-25-025 shows 41.5 nm in width. Except for sample B150-25-180, all imprinted patterns deviated from the mold. The fidelity pattern of sample B150-25-180 is due to the plastic deformation during the imprinting process.

As shown in Figs. 5(a)–5(c), sample A150-25-130 has a shallow trench; the sidewall of sample B150-25-130 tapers in the tips, but sample B150-25-180 shows a steeper profile. The differences in imprinting results are caused by the process parameters and the properties of HSQ. In the case of

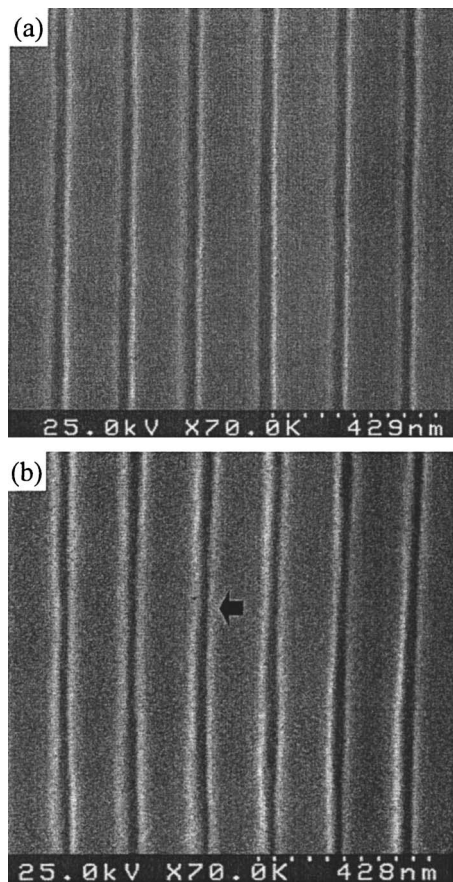


FIG. 6. Pattern degradations of sample B050-25-025. (a) As imprinted, (b) after 4 days of aging.

sample B150-25-180, after being prebaked at 150 °C, the sample was imprinted at 180 °C under 2.5 MPa. Heating to 180 °C makes HSQ further transfer into network-type, and applying pressure helps the HSQ to adjust its configuration to conform to the mold pattern. However, for sample B150-25-130, the imprinting temperature is only 130 °C; the temperature seems insufficient to afford HSQ the network structure to exhibit plastic deformation during the imprint. As a result, the imprinted linewidth and depth rebound after releasing the pressure, and the result is narrower and shallower lines. According to the experimental results and discussion, the process parameters for making a high-fidelity replication is prebaking at 150 °C for 3 min and imprinting at 180 °C under a pressure of 2.5 MPa for 2 min, as in sample B150-25-180.

The room-temperature aging effects on pattern degradation of imprinted HSQ is shown in Figs. 6 and 7. Figure 6(a) is the SEM top view of sample B050-25-025 observed within one day; Fig. 6(b) is the SEM micrograph taken after four days of aging. After aging in room temperature for four days, the line shape of sample B050-25-025 is heavily distorted. The linewidth marked by an arrow in Fig. 6(b) varies from 51.2 to 36.2 nm. Figure 7(a) is the SEM of sample B150-25-180 observed within one day, and Fig. 7(b) is the SEM micrograph of the sample aged at room temperature for 20 days. The average linewidth of sample B150-25-180 is

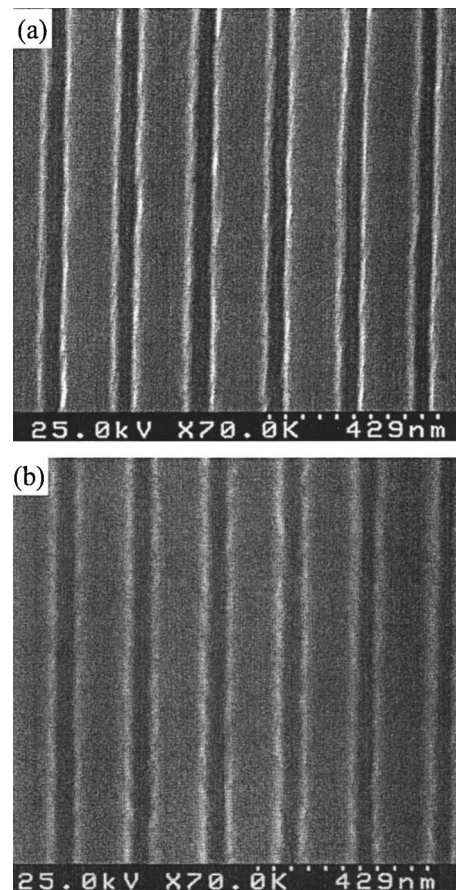


FIG. 7. Pattern degradations of sample B150-25-180. (a) As imprinted, (b) after 20 days of aging.

slightly deviated from 58.1 nm (before aging) to 59.8 nm (after 20 days of room-temperature aging). Again, the non-degradation of sample B150-25-180 is due to its plastic deformation during imprinting, which correlated to chemical structures and mechanical properties.

As mentioned above, sample B050 shows low viscosity and high viscous response; this means it is not easy for plastic deformation to occur during imprinting. In other words, the indented areas may partially rebound after releasing the imprint pressure for sample B050-25-025. However, sample B050 has more cage-like Si–O bonding. For cage-like HSQ, the movements of molecules are determined only by the oligomer itself. This means that the rebounding of sample B050-25-025 is random and unconstrained by neighboring molecules. In this mechanism, the rebounding of HSQ is expected to occur randomly and to result in inhomogeneous dilation or shrinkage of imprint patterns. This is why after four days of aging at room temperature, the line shapes of sample B050-25-025 become heavily distorted and contribute to the variation of line width. It has been proven that the network Si–O bonding is promoted after treatment at 180 °C. Forming network bonds can also unite individual HSQ molecules to form a stable three-dimensional structure. As the case of sample B150-25-180, the formation of network bonding makes the sample more stable than the cage-

like type, and line pattern unchanges during room-temperature aging. So, the shape and line width of network-type HSQ is not easy to change. This is why the linewidth and line shape are both the same for sample B150-25-180 with or without aging at room temperature for 20 days, as shown in Fig. 7.

IV. CONCLUSIONS

In this study, we focus on the effects of process parameters on the properties of HSQ, pattern embossing into HSQ films, and the pattern degradation of HSQ for room-temperature aging. The FTIR results show that the network-type bonding is promoted by dilution with MIBK and increased baking temperatures from 50 °C to 180 °C. The indentation test results show that sample B180 has a lower hardness and modulus, less viscous response, and higher plastic deformation than that of samples A150 and B050. The plastic deformation of sample B150-25-180 during the imprinting process gives fidelity pattern replication. The formation of network bonding makes HSQ more stable than cage-

like-type HSQ. As a result, sample B150-25-180 shows no degradation in replication patterns after aging at room temperature for 20 days.

ACKNOWLEDGMENTS

This paper was supported by the National Science Council of Taiwan, ROC, under Contract No. NSC-93-2215-E-007-021. The authors would also like to thank Dow Corning Taiwan, Inc. for supplying the HSQ and MIBK chemicals.

¹S. Y. Chou, P. R. Krauss, and P. J. Renstrom, *J. Vac. Sci. Technol. B* **14**, 4129 (1996).

²P. Fairly, *Technol. Rev.* **106**, 42 (2003).

³T. Morita, K. Watanabe, R. Kometani, K. Kanda, Y. Haruyama, T. Kaito, J. Fujita, M. Ishida, Y. Ochiai, T. Tajima, and S. Matsui, *Jpn. J. Appl. Phys., Part 1* **42**, 3874 (2003).

⁴S. Matsui, Y. Igaku, H. Ishigaki, J. Fujita, M. Ishida, Y. Ochiai, H. Namatsu, and M. Komuro, *J. Vac. Sci. Technol. B* **21**, 688 (2003).

⁵A. K. Sikder and A. Kumar, *J. Electron. Mater.* **31**, 1016 (2002).

⁶A. K. Sikder, A. Kumar, S. Thagella, and J. Yota, *J. Mater. Res.* **19**, 996 (2004).

⁷M. L. Oyen and R. F. Cook, *J. Mater. Res.* **18**, 139 (2003).

⁸W. Henschel, Y. M. Georgiev, and H. Kurz, *J. Vac. Sci. Technol. B* **21**, 2018 (2003).